ChemComm

COMMUNICATION

View Article Online
View Journal | View Issue



Cite this: *Chem. Commun.*, 2015, **51**, 330

Received 13th October 2014,
Accepted 5th November 2014

DOI: 10.1039/c4cc08072f

www.rsc.org/chemcomm

# Tuning intramolecular electron and energy transfer processes in novel conjugates of $La_2@C_{80}$ and electron accepting subphthalocyanines†

Lai Feng,*[ab] Marc Rudolf,[c] Olga Trukhina,[de] Zdenek Slanina,[f] Filip Uhlik,[g] Xing Lu,[h] Tomas Torres,*[de] Dirk M. Guldi*[c] and Takeshi Akasaka*[bhij]

**A series of two conjugates with $La_2@C_{80}$ and subphthalocyanine (SubPc) have been prepared and characterized by means of cyclic voltammetry, absorption, fluorescence, and femtosecond resolved transient absorption spectroscopy. The strong electron-donating character of $La_2@C_{80}$ is essential to power an intramolecular electron-transfer in the $La_2@C_{80}$–SubPc conjugates upon photoexcitation.**

Mimicking photosynthesis has been of a great interest owing to the increasing need for an efficient and sustainable conversion of solar energy.[1,2] One of the key factors in the reproduction of natural photosynthesis is to understand electron-transfer events between different electron donors and acceptors of the photosynthetic apparatus. Importantly, the nature of electron donors and acceptors determines the magnitude of electron transfer and, in turn, affects the overall yield of photosynthesis. Extensive studies have been carried out to design, to synthesize, and to probe electron donor and electron acceptor materials with improved performances in solar energy conversion.[3,4] For photovoltaic applications, fullerenes stand out among the myriad of electron accepting materials.[5] Owing to their unique structural and redox features, fullerenes have been widely integrated into a wide facet of electron donor–acceptor systems.[6] It is also well known that the use of empty fullerenes $C_{60}$ and $C_{70}$ as electron donors in molecular photovoltaics is limited by their poor electron-donating ability. The generation of radical cations of, for example, $C_{60}$ or $C_{70}$ requires rather harsh conditions.[7] Up to now, none of them have been employed as electron donors either in artificial photosynthesis or in photovoltaics.

Filling empty fullerenes with metals or metallic clusters affords endohedral metallofullerenes (EMFs), whose physical, chemical and electrochemical properties are different from those of empty fullerenes.[8] For example, $La@C_{82}$, $M_2@C_{80}$ (M = La, Ce), and $M_3N@C_{80}$ (M = Sc, Lu) undergo easier oxidations and feature stronger absorption throughout the visible part of the solar spectrum when compared to $C_{60}$ and $C_{70}$. These characteristics render EMFs p-type materials for photovoltaics. Very recently, the idea of using EMFs as electron donors has been verified in photophysical assays with $Lu_3N@C_{80}$ or $La_2@C_{80}$ as the electron donor and PDI or TCAQ as the electron acceptor, respectively.[9,10]

Subphthalocyanines (SubPcs) are aromatic chromophores, which absorb light throughout most of the visible part of the spectrum featuring (i) high extinction coefficients, (ii) excitation energies above 2.0 eV, and (iii) low reorganization energies in electron transfer reactions.[11] Importantly, they do not aggregate owing to their conical shape and are known as strong fluorophores. SubPcs bearing on their periphery electron-withdrawing substituents are well-known electron acceptors.[11b] Thus, electron-deficient SubPcs have been considered as promising complements to fullerenes.

In the present work, we report on the synthesis and the properties of conjugates **1a** and **1b** (Scheme 1) that comprise $La_2@C_{80}$ as electron donor and (dodecafluoro)/hexa(pentylsulfonyl)SubPc as electron acceptors. We will demonstrate that, despite negligible interactions in the ground-state, electron-transfer events occur between SubPc and $La_2@C_{80}$ in the excited state. However, in conjugates **2a** and **2b**, only energy transfer events take place.

[a] *College of Physics, Optoelectronics and Energy & Collaborative Innovation Center of Suzhou Nano Science and Technology, Soochow University, 215006 Suzhou, China. E-mail: fenglai@suda.edu.cn*
[b] *Life Science Center of Tsukuba Advanced Research Alliance, University of Tsukuba, 305-8577 Tsukuba, Japan. E-mail: akasaka@tara.tsukuba.ac.jp*
[c] *Department of Chemistry and Pharmacy & Interdisciplinary Center for Molecular Materials, Friedrich-Alexander-Universität Erlangen-Nürnberg, 91058 Erlangen, Germany. E-mail: dirk.guldi@fau.de*
[d] *Department of Organic Chemistry, Autonoma University of Madrid, 28049 Madrid, Spain. E-mail: tomas.torres@uam.es*
[e] *IMDEA Nanoscience, 9 Faraday, 28049 Madrid, Spain*
[f] *Department of Chemistry and Biochemistry, National Chung-Cheng University, 62117 Chia-Yi, Taiwan, Republic of China*
[g] *Department of Physical and Macromolecular Chemistry, Charles University in Prague, 6 Albertov, 12843 Praha 2, Czech Republic*
[h] *College of Materials Science and Engineering, Huazhong University of Science and Technology, 430074 Wuhan, China*
[i] *Foundation for Advancement of International Science, 305-0821 Tsukuba, Japan*
[j] *Department of Chemistry, Tokyo Gakugei University, 184-8501 Koganei, Japan*

† Electronic supplementary information (ESI) available: Experimental details, complete characterizations of **1a**, **1b**, and selected transient absorption spectra. See DOI: 10.1039/c4cc08072f

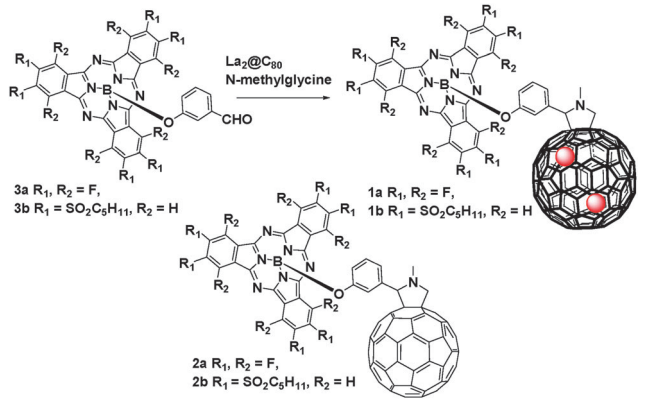


Scheme 1 Synthesis of $La_2@C_{80}$–SubPc (**1a** and **1b**) from subphthalocyanines (**3a**, **3b**).

Conjugates **1a**, **1b** were synthesized according to the procedure previously reported for **2a**.[12] Briefly, **1a**, **1b** were obtained in 25% or less *via* Prato reaction of $La_2@C_{80}$ and SubPc **3a**, **b**[13] (Scheme 1). The formation of **1a** or **1b** as major products was revealed by HPLC and they were isolated *via* a multi-step HPLC procedure (Fig. S1–S3, ESI†).[14] The compositions of **1a** and **1b** were confirmed using MALDI-TOF mass spectrometry (Fig. S5–S7, ESI†).

To shed light onto the structural feature of **1a**, VT $^1$H NMR studies were conducted. As shown in Fig. S8 (ESI†), the $^1$H NMR spectrum measured at 283 K exhibits two sets of signals: those originating from pyrrolidine protons at 5–2 ppm and those from phenyl protons at 8–5.5 ppm, indicating the presence of at least two conformers of **1a** in a 3 : 1 ratio. In each set, a pair of doublets, which are assigned to the geminal protons on the pyrrolidine, is discernible. Confirmation for this assignment was obtained by COSY experiments, revealing a reasonable cross-coupling relationship between the doublets (Fig. S9, ESI†). In addition, the chemical shifts as well as the chemical shift differences ($\Delta\delta$ = 1.2 to 1.3 ppm) of these geminal protons are in a good agreement with those reported previously.[15] An increase of the temperature from 283 to 313 K resulted only in a broadening of the NMR signals in **1a** (Fig. S8, ESI†) ruling out the possibility of conformational conversion in this temperature range. Characterization of **1b** using $^1$H NMR was, however, hampered by the small amounts of the isolated material and its poor stability.

To further investigate the structural and electronic features of **1a**, DFT-calculations were performed using a *Gaussian 09* package.[16] Owing to the [5,6]-addition pattern and the unsymmetrical pyrrolidine substitution, **1a** adopts at most four different conformations – Fig. S13 (ESI†). Among them, conformer **I**, in which both, the pyrrolidine and the substituted phenoxy unit, are approaching a 5-member ring, has the lowest formation energy (Table S1, ESI†) at the M06-2X/3-21G ~ 6-31G* ~ sdd level.[17–19] In comparison, conformer **II**, in which both the pyrrolidine and the substituted phenoxy group are aligned close to a 6-member ring, is 2.3–3.3 kcal mol$^{-1}$ less stable than conformer **I**. Conformers **III** and **IV** possess the least stability, namely 5.3 kcal mol$^{-1}$ less than conformer **I**. Therefore, we hypothesize the presence of conformers **I** and **II** in purified **1a** with a ratio of 3 : 1.

Electrochemical studies with **1a** and **2a** were carried out by means of CV and DPV. In the range from −2.0 to 1.2 V, **2a** reveals four reversible one-electron reductions at −1.06, −1.18, −1.57, and −1.79 V and two irreversible one-electron oxidations at +0.99 and +1.08 V (Table 1 and Fig. S12, ESI†). The first oxidation, and the first and third reductions are $C_{60}$ centered, while the second oxidation, and the second and forth reductions are centered on SubPc. As for **1a**, the electrochemical patterns of the [5,6]-pyrrolidine $La_2@C_{80}$ and perfluorinated SubPc are clearly distinguishable.[12,15] In particular, the first and second reductions, which are seen as a one-electron process at −0.47 and −1.12 V, coincide well with the reductions of $La_2@C_{80}$ and SubPc, respectively. The third reduction at −1.80 V appears as a two-electron process, involving the second reduction of $La_2@C_{80}$ and the second reduction of SubPc. In addition, three oxidations are visible. The first and second are fully reversible one-electron processes, which agree well with those of $La_2@C_{80}$. The third oxidation is a two-electron process, corresponding to the first oxidation of SubPc and the third oxidation of $La_2@C_{80}$. Our electrochemical assays point to the fact that ground state interactions between the electroactive constituents of **1a** are negligible. The remarkable oxidative features of **1a** underline the strong electron donor character of $La_2@C_{80}$, which is lacking in $C_{60}$ in **2a**.

Table 1 Redox potentials[a] of $La_2@C_{80}$–SubPc conjugate **1a** and reference compounds, $E_p$ *vs.* Fc/Fc$^+$, V

| | $E^3_{ox}$ | $E^2_{ox}$ | $E^1_{ox}$ | $E^1_{red}$ | $E^2_{red}$ | $E^3_{red}$ | $E^4_{red}$ |
|---|---|---|---|---|---|---|---|
| **1a** | 0.97[b] | 0.58 | 0.20 | −0.47 | −1.12 | −1.80[b] | |
| **2a** | | 1.08 | 0.99 | −1.06 | −1.18 | −1.57 | −1.79 |
| **4**[c] | 1.00[b] | 0.59 | 0.20 | −0.44 | −1.70 | −2.13 | |

**4** = [5,6]-pyrrolidine $La_2@C_{80}$:$La_2@C_{80}$–NTrt (Trt = triphenylmethyl). [a] Values obtained from DPVs. [b] Two-electron process. [c] Data from ref. 15.

Complementary DFT-calculations further underline the electrochemical data. As shown in Fig. S14 (ESI†), the calculated HOMO of **1a** is mainly delocalized on $La_2@C_{80}$, while the LUMO and LUMO + 1 are localized on the endohedral $La_2$ cluster and on the perfluorinated SubPc, respectively.

To gain further insight into the ground state features of **1a–b**, we turned to absorption spectroscopy. At a first glance, the absorption spectrum of **1a–b** is best described as a simple superimposition of the spectra of the individual components, namely SubPc and [5,6]-pyrrolidine $La_2@C_{80}$ (Fig. S10 and S11, ESI†). Detailed comparison between **1a** and **1b** suggests that the absorption maxima of **1b** are 4 nm red-shifted relative to that of **1a**, thus, confirming the stronger electron–acceptor properties of sulfonated SubPcs than of the fluorinated one. Despite the presence of [5,6]-pyrrolidine $La_2@C_{80}$, the absorption maximum of SubPc undergoes no shift as compared with that of SubPc **3a** and **3b**, indicating the lack of ground-state interaction between the individual components.

In fluorescence experiments, a solvent independent fluorescence quantum yield of 0.17 was noted for **3a**. In stark contrast, fluorescence assays with **1a** point to a rather marked quenching with fluorescence quantum yields of 0.005 (toluene), 0.006 (THF), and 0.006 (benzonitrile).

To attribute our spectral observation, spectroelectrochemical experiments on $(F_{12}SubPc)^{\bullet-}$ and $((SO_2C_5H_{11})_6SubPc)^{\bullet-}$ as well as $(La_2@C_{80})^{\bullet+}$ were deemed important – Fig. S15 (ESI†). On the one hand, the differential absorption spectra of the electrochemically

reduced **3a** reveal two broad features with maxima at 455 and 655 nm, which are accompanied by shoulders at around 475 and 610 nm, as well as a minimum at 570 nm. Upon spectroelectrochemical reduction of **3b**, spectral characteristics including maxima at 480, 545, 620, and 735 nm complemented by minima at 534 and 581 nm evolved. Notably, pulse radiolytic reductions with **3a** or **3b** in deaerated toluene/2-propanol/acetone mixtures (8 : 1 : 1 v/v) results in quantitatively similar spectra with characteristic fingerprints at 610 and 620 nm, respectively. On the other hand, a characteristic maximum at 900 nm and a broad near infrared tail evolve as spectroscopic characteristics upon spectroelectrochemical oxidation of **4**.

Insights into the excited state deactivation in **4**, **3a**, **3b**, **2a**, **2b**, **1a**, and **1b**, in general, and into the corresponding photoproducts, in particular, came from transient absorption measurements following femtosecond and nanosecond excitation. Excitation of **4** at 387 nm leads to the population of the $La_2@C_{80}$ singlet excited state (1.4 ± 0.2 eV), which features ground state bleaching at 465 nm and well-resolved fine structure with maxima at 516, 466, 614, 735, 800, and 900 nm. The latter is subject to a fast intersystem crossing – 60 ± 30 ps – to the triplet manifold due to the presence of the $(La_2)^{6+}$ cluster, which promotes efficient spin–orbit coupling. Following the singlet excited state decay, a weak and broad absorption in the 800–1200 nm region, along with broad features that taper at 550 nm, are discernible. These features relate to the $La_2@C_{80}$ triplet excited state (1.0 ± 0.1 eV).

$F_{12}$SubPc **3a** reveals upon excitation at 530 nm differential absorption changes, which include transient maxima at 440 and 600 nm as well as transient minima at 514, 575, and 635 nm – Fig. S16 (ESI†). In addition, a broad near-infrared feature spans from 650 to 1200 nm, which peaks around 710 nm. These features relate to the singlet excited state (2.16 eV) of **3a**, which transforms with 1.9 ± 0.1 ns into the corresponding triplet excited state (1.4 eV). Transient absorption spectra of the latter maximize at 470 and 610 nm and minimize at 532 and 570 nm.

Commencing with the conclusion of the 530 nm excitation, SubPc **3b** reveals differential absorption changes in the form of transient maxima at 424, 474, 623, 660 nm, a broad tail extending far into the near infrared, as well as transient minima at 533 and 583 nm – Fig. S17 (ESI†). These SubPc singlet excited state (2.12 eV) related transient absorption features undergo intersystem crossing to the corresponding triplet excited state (1.4 eV), which exhibits a broad transient in the visible part of the spectrum. The latter maximizes at 470 and 620 nm and minimizes at 533 and 583 nm. Owing to the presence of sulfur, which facilitates spin–orbit coupling, the intersystem crossing is accelerated relative to what is seen for **3a** with lifetimes of 1220 ± 20 ps, 420 ± 10 ps, 415 ± 10 ps in toluene, THF, and benzonitrile, respectively.

Conjugate **1a** gives rise upon 530 nm excitation to differential absorption changes in the form of transient maxima at 450, 600, and 720 nm as well as transient minima at 575 and 635 nm – Fig. 1. In line with the reference experiments, namely with **3a**, we assign these changes to the $F_{12}$SubPc singlet exited state. Instead of seeing the slow intersystem crossing to the SubPc triplet state, the SubPc singlet excited state decays ultrafast with lifetimes of 3.0 ± 0.4 ps (toluene), 2.2 ± 0.2 ps (THF), and 2.0 ± 0.2 ps (benzonitrile). Simultaneously, new transitions develop in the visible and near-infrared regions.

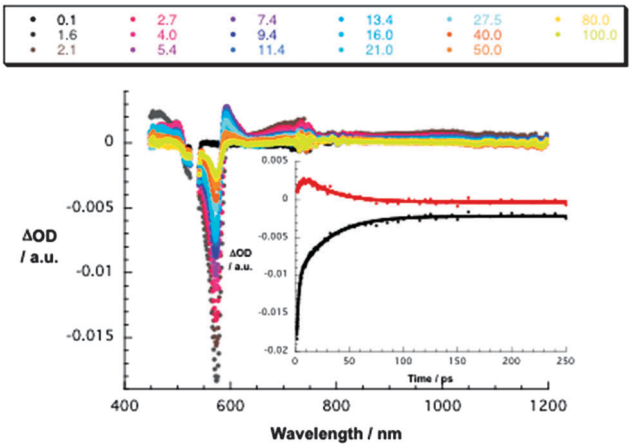


Fig. 1 Differential absorption spectra (visible and near-infrared) obtained upon femtosecond flash photolysis (530 nm) of **1a** ($10^{-5}$ M) in argon-saturated THF with several time delays between 0.1 and 100 ps at room temperature. Inset: time-absorption profiles of the spectra shown at the top at 573 and 592 nm monitoring the charge separation and the charge recombination.

Importantly, the new transients do not match the signature of the SubPc triplet excited state. Instead, maxima at 480 and 590 nm as well as minima at 515 and 570 nm are discernible. Please note that these features bear great resemblance to the pulse radiolytic findings in the context of reducing SubPc and, as such, relate to its π-radical anion – $(F_{12}SubPc)^{\bullet -}$. In the near-infrared region, a broad tail is attributable to the $La_2@C_{80}$ π-radical cation, that is, $(La_2@C_{80})^{\bullet +}$. Taking the aforementioned into consideration, we conclude that an energetically low lying radical ion pair state (1.32 eV), namely $(La_2@C_{80})^{\bullet +}$–$(F_{12}SubPc)^{\bullet -}$, is formed. Both fingerprints served as reliable probes to determine the lifetime of the metastable $(La_2@C_{80})^{\bullet +}$–$(F_{12}SubPc)^{\bullet -}$ radical ion pair state. All decays were well fitted by a single exponential fitting function throughout the femtosecond time scale. In particular, lifetimes of 34 ± 2 ps (toluene), 32 ± 2 ps (THF), and 35 ± 2 ps (benzonitrile) were derived.

Singlet oxygen quantum yields for **1a** are as low as 0.010 in THF and support the assignment that any other state than the $F_{12}$SubPc triplet excited state evolves as the product of charge recombination. Please note the singlet oxygen yields in **3a** of 0.31 (toluene), 0.10 (THF), and 0.35 (benzonitrile).

Laser excitation of **1b** in benzonitrile at 568 nm results immediately after excitation in differential absorption maxima at 485 and 623 nm and a minimum at 583 nm – Fig. S18 (ESI†). Although these transient features relate to the singlet excited state of SubPc they decay ultrafast with a lifetime of 1.4 ± 0.1 ps. New transients evolve, which maximize at 480 and 610 nm and minimize 583 nm. A spectral comparison with the results from the spectroelectrochemical/pulse radiolytic investigations supports the notion that the new transients are attributed to the π-radical anion – $((SO_2C_5H_{11})_6SubPc)^{\bullet -}$. Taking the aforementioned into consideration, we postulate an electron transfer from $La_2@C_{80}$ to the SubPc singlet excited state to afford $(La_2@C_{80})^{\bullet +}$–$((SO_2C_5H_{11})_6SubPc)^{\bullet -}$ (1.36 eV). It is worth mentioning that the detection of $(La_2@C_{80})^{\bullet +}$ in the near infrared is hampered by the thermal decomposition of SubPc. This is seen to form a product with absorptions in the 700–850 nm range.

 

Nevertheless, the metastable $(La_2@C_{80})^{\bullet+}$–$((SO_2C_5H_{11})_6SubPc)^{\bullet-}$ radical ion pair state decays with 28 ± 2 ps to the singlet ground state.

Likewise, 530 nm excitation of $F_{12}SubPc$-$C_{60}$ **2a** results in the exclusive formation of the SubPc singlet excited state – Fig. S19 (ESI†). In particular, transient maxima at 450, 600, and 720 nm as well as transient minima at 515, 575, and 635 nm are formed and decay rapidly with 1.5 ± 0.3 ps (toluene), 1.5 ± 0.3 ps (THF), and 1.4 ± 0.3 ps (benzonitrile). As the SubPc singlet excited state decay comes to an end a broad near-infrared transient, which maximizes at 910 nm, is noted, suggesting a $C_{60}$ singlet excited state. Interestingly, we did not find the characteristic $C_{60}$ triplet feature at 700 nm at the end of the $C_{60}$ singlet excited state deactivation. In contrast, maxima at 470 and 615 nm as well as a minimum at 575 nm were found, pointing to the SubPc triplet excited state.[12] From this we infer that the $C_{60}$ triplet excited state (1.5 eV) undergoes a thermodynamically allowed transfer of triplet excited state energy to SubPc (1.4 eV). The kinetics at the 470 and 615 nm maxima further furnishes the kinetic assignment, namely the rate-determining step in the SubPc triplet excited state formation is the $C_{60}$ centered intersystem crossing. A global analysis reveals kinetics that are very similar (1.6 ± 0.1 ns) to that of the inherent intersystem crossing dynamics seen for $C_{60}$. In this context, it is reassuring that the transients seen at the end of the femtosecond experiments matches that at the beginning of the nanosecond experiment. Moreover, maxima at 470 and 610 nm, minima at 532 and 570 nm, and an excited state lifetime of 36 μs without oxygen perfectly agree with the SubPc triplet excited state of **3a**. Likewise, singlet oxygen quantum yields of **2a** were found to be as high as 0.28 (toluene), 0.13 (THF), and 0.41 (benzonitrile) and support the assignment that the triplet excited state evolves as the product of charge recombination. Please note that the singlet oxygen yields in **3a** are as high as 0.35.

When turning to **2b**, excitation at 530 nm is accompanied by the formation of its singlet excited state – Fig. S20 (ESI†). Evidence stems from monitoring maxima at 427, 474, 623, and 660 nm and minima at 535 and 585 nm. These decay in the presence of $C_{60}$ rapidly with 1.5 ± 0.3 ps (toluene), 1.5 ± 0.3 ps (THF), and 1.4 ± 0.3 ps (benzonitrile) to form accordingly the $C_{60}$ singlet excited state with its 910 nm maximum. Like for **2a**, we did not find the characteristic $C_{60}$ triplet feature. Instead, maxima at 470 and 625 nm as well as minima at 535 and 585 nm of the SubPc triplet excited state were concluded. In other words, the triplet excited state of SubPc (1.4 eV) evolves from a thermodynamically allowed transfer of triplet excited state. The kinetics at the 470 and 625 nm maxima and the 585 nm minimum document that the rate-determining step is the $C_{60}$ centered intersystem crossing (1.6 ± 0.1 ns). In the absence of oxygen, the SubPc triplet excited state lifetime is 20 ± 5 μs in agreement with what was found for **3b**.

Electron accepting SubPcs have been used in combination with $La_2@C_{80}$ to prepare a series of novel $La_2@C_{80}$–SubPc electron donor–acceptor conjugates to mimic the photosynthetic apparatus. Our results in terms of electrochemical and steady-state absorption reveal no appreciable electronic interactions between SubPc and $La_2@C_{80}$ in the ground state. This changed in the excited state, where an intramolecular electron-transfer evolves from $La_2@C_{80}$ to photoexcited SubPc. In comparison, reference conjugates of $C_{60}$ and SubPcs feature only a singlet–singlet energy transfer from SubPc to $C_{60}$. Thus, replacing $C_{60}$ by $La_2@C_{80}$ provides a promising way to tune energy-transfer *versus* electron-transfer. Furthermore, considering the short separations between the electron donors and acceptors, optimizing the charge-separated state lifetimes seems achievable *via* the tailored design of linkers between $La_2@C_{80}$ and SubPc.

This work is financially supported by the NSFC (51372158), the NSF of Jiangsu Province (BK2012611), the Jiangsu Specially Appointed Professor Program (SR10800113), Priority Academic Program Development of Jiangsu Higher Education Institutions (PAPD), the Project for Jiangsu Scientific and Technological Innovation Team (2013), Spanish MEC and MICINN (CTQ2011-24187/BQU and PRI-PIBUS-2011-1128), the Deutsche Forschungsgemeinschaft (GU 517/14-1) and the Comunidad de Madrid (S2013/MIT-2841, FOTOCARBON).

## Notes and references

1 A. A. Boghossian, M. H. Ham, J. H. Choi and M. S. Strano, *Energy Environ. Sci.*, 2011, **4**, 3834–3843.
2 (*a*) S. Hammes-Schiffer, *Acc. Chem. Res.*, 2009, **42**, 1881–1889; (*b*) M. R. Wasielewski, *Chem. Rev.*, 1992, **92**, 435–461.
3 G. de la Torre, G. Bottari, M. Sekita, A. Hausmann, D. M. Guldi and T. Torres, *Chem. Soc. Rev.*, 2013, **42**, 8049–8105.
4 G. Bottari, G. de la Torre, D. M. Guldi and T. Torres, *Chem. Rev.*, 2010, **110**, 6768–6816.
5 S. Kirner, M. Sekita and D. M. Guldi, *Adv. Mater.*, 2014, **26**, 1482–1493.
6 (*a*) J. L. Delgado, P. A. Bouit, S. Filippone, M. A. Herranz and N. Martín, *Chem. Commun.*, 2010, **46**, 4853–4865; (*b*) D. M. Guldi, *Chem. Soc. Rev.*, 2002, **31**, 22–36.
7 (*a*) K. Ohkubo, J. Ortiz, L. Martin-Gomis, F. Fernandez-Lazaro, A. Sastre-Santos and S. Fukuzumi, *Chem. Commun.*, 2007, 589–591; (*b*) C. A. Reed, K. C. Kim, R. D. Bolskar and L. J. Mueller, *Science*, 2000, **289**, 101–104; (*c*) S. Fukuzumi, H. Mori, H. Imahori, T. Suenobu, Y. Araki, O. Ito and K. M. J. Kadish, *J. Am. Chem. Soc.*, 2001, **123**, 12458–12465.
8 (*a*) A. A. Popov, S. Yang and L. Dunsch, *Chem. Rev.*, 2013, **113**, 5989–6113; (*b*) X. Lu, L. Feng, T. Akasaka and S. Nagase, *Chem. Soc. Rev.*, 2012, **41**, 7723–7760.
9 (*a*) M. Rudolf, L. Feng, Z. Slanina, T. Akasaka, S. Nagase and D. M. Guldi, *J. Am. Chem. Soc.*, 2013, **135**, 11165–11174; (*b*) L. Feng, M. Rudolf, S. Wolfrum, A. Troeger, Z. Slanina, T. Akasaka, S. Nagase, N. Martín, T. Ameri, C. J. Brabec and D. M. Guldi, *J. Am. Chem. Soc.*, 2012, **134**, 12190–12197.
10 Y. Takano, S. Obuchi, N. Mizorogi, R. García, M. A. Herranz, M. Rudolf, D. M. Guldi, N. Martín, S. Nagase and T. Akasaka, *J. Am. Chem. Soc.*, 2012, **134**, 19401–19408.
11 (*a*) C. G. Claessens, D. Gonzalez-Rodriguez, M. S. Rodriguez-Morgade, A. Medina and T. Torres, *Chem. Rev.*, 2014, **114**, 2192–2277; (*b*) C. Romero-Nieto, A. Medina, A. Molina-Ontoria, C. G. Claessens, L. Echegoyen, N. Martin, T. Torres and D. M. Guldi, *Chem. Commun.*, 2012, **48**, 4953–4955.
12 D. Gonzalez-Rodriguez, T. Torres, D. M. Guldi, J. Rivera, M. A. Herranz and L. Echegoyen, *J. Am. Chem. Soc.*, 2004, **126**, 6301–6313.
13 M. Ince, A. Medina, J. H. Yum, A. Yella, C. G. Claessens, M. V. Martinez-Diaz, M. Graetzel, M. K. Nazeeruddin and T. Torres, *Chem. – Eur. J.*, 2014, **20**, 2016–2021.
14 In the reaction mixture, besides **1a**, a minor product **1a′** was also isolated and identified as a [6,6]-pyrrolidine adduct using MALDI-TOF mass and UV-vis-NIR absorption spectra (Fig. S6 and S9, ESI†).
15 (*a*) M. Yamada, M. Okamura, S. Sato, I. C. Someya, N. Mizorogi, T. Tsuchiya, T. Akasaka, T. Kato and S. Nagase, *Chem. – Eur. J.*, 2009, **15**, 10533–10542; (*b*) T. Cai, Z. Ge, E. B. Lezzi, T. E. Glass, K. Harich, H. W. Gibson and H. C. Dorn, *Chem. Commun.*, 2005, 3594–3596.
16 M. J. Frisch, *et al.*, *GAUSSIAN 09, Revision A. 02*, Gaussian Inc., Wallingford, CT, 2009.
17 Y. Zhao and D. G. Truhlar, *Theor. Chem. Acc.*, 2008, **120**, 215–241.
18 X. Y. Cao and M. Dolg, *THEOCHEM*, 2002, **581**, 139–147.
19 A. D. Becke, *J. Chem. Phys.*, 1993, **98**, 5648–5652.